FULL PAPER

Dalton
www.rsc.org/dalton

Biologically relevant mono- and di-nuclear manganese II/III/IV complexes of mononegative pentadentate ligands †

Carole Baffert,[a] Marie-Nöelle Collomb,[a] Alain Deronzier,[a] Sanne Kjærgaard-Knudsen,[b] Jean-Marc Latour,[c] Kirsten H. Lund,[b] Christine J. McKenzie,*[b] Martin Mortensen,[b] Lars Preuss Nielsen[b] and Niels Thorup[d]

[a] *Laboratoire d'Electrochimie Organique et de Photochimie Rédox CNRS UMR 5630, Université Joseph Fourier, 38041 Grenoble, France*

[b] *Department of Chemistry, University of Southern Denmark, Odense Campus, 5230 Odense M, Denmark*

[c] *Laboratoire de Physicochimie des Métaux en Biologie, Département de Biologie Moléculaire et Structurale, CEA/Grenoble, 38054 Grenoble Cedex 9, France*

[d] *Department of Chemistry, Technical University of Denmark, DK-2800 Lyngby, Denmark*

Received 21st January 2003, Accepted 28th February 2003
First published as an Advance Article on the web 18th March 2003

Manganese(II) complexes of mononegative pentadentate N_4O ligands $[Mn_2(mgbpen)_2(H_2O)_2](ClO_4)_2$ (**1**), (mgbpen$^-$ = *N*-methyl-*N′*-glycyl-*N*,*N′*-bis(2-pyridylmethyl)ethane-1,2-diamine) and $[Mn_2(bzgbpen)_2(H_2O)_2](ClO_4)_2$ (**2**), (bzgbpen$^-$ = *N*-benzyl-*N′*-glycyl-*N*,*N′*-bis(2-pyridylmethyl)ethane-1,2-diamine) have been prepared. The crystal structure of the Mn(II)–aqua complex of **1**, shows it to be dimeric *via* (μ-κ*O*)-bridging through one carboxylate oxygen atom of each of the two ligands. The non-coordinated carboxylate oxygen atoms are H-bonded to the water ligands on the adjacent Mn ion. The magnetic coupling interaction is weak and antiferromagnetic, $J = -1.3(1)$ cm^{-1}. The dimeric structures of **1** and **2** are retained in solution and can exist in the gas phase. Complexes **1** and **2** are air stable but can be oxidised by ^{t}BuOOH to give unstable mononuclear Mn(III) complexes, or oxo-bridged dimanganese(III) and di-μ-oxo-dimanganese(IV) complexes, depending on solvent. The $[Mn(III)–OR]^+$, R = H or CH_3 complexes are generated in water or methanol, respectively, and are potentially useful spectroscopic models for active Mn–lipoxygenases. In acetonitrile, di-μ-oxo-dimanganese(IV) complexes are the highest oxidation state products detected, and these are formed *via* shorter-lived intermediate μ-oxo-dimanganese(III) compounds. The rate of formation of the various oxidized products is slower in the case of the bzgbpen$^-$ systems which contains a bulkier non-coordinating arm. The oxidised complexes were characterised by UV-visible spectroscopy, ESI mass spectrometry and cyclic voltammetry. In addition, III–IV and II–III species were electrochemically generated. Thus the new mononegative pentadentate ligand systems display significant flexibility in the range of Mn oxidation states and species of biological relevance that are accessible: A series of dinuclear compounds with different structures in the five oxidation levels between II–II and IV–IV has been identified. No solid state structures were obtained for high oxidation state species, however it is assumed that in the oxo-bridged compounds the carboxylate groups are terminally ligated in contrast to the starting Mn(II) complexes. Thus the system represents examples of limiting structures in the "carboxylate shift" mechanism proposed to be important in non-heme H_2O and O_2 activation processes.

Introduction

Manganese is involved in biological redox reactions involving water, peroxide and dioxygen where oxidation states II, III and IV are implicated in mono-, di- and multi-nuclear centres. These include the oxygen evolving center (OEC) of photosystem II,[1] catalases,[2] manganese ribonucleotide reductase,[3] superoxide dismutases,[4] and peroxidases.[5,6] Recently a manganese lipoxygenase (Mn–LOX) isolated from the fungus *Gäunnomyces gramminis* was cloned and sequenced.[7,8] Significant homology to the mammalian Fe–LOX family was revealed with a good alignment, for the proposed mononuclear manganese binding site. The most likely metal donors for Mn–LOX are His294, His297, His478 and Asn482 and the C terminus carboxylate (valine). Thus the protein in Mn–LOX, similar to the Fe–LOXs, is proposed to furnish a pentadentate mononegatively-charged coordination site. Likewise, cycling between E–M(II)[H] and E–M(III) states, where the latter functions as H-atom abstractor towards the substrate, is the rate determining step in the proposed enzymatic mechanism of Mn–lipoxygenase. The function in the Fe–LOXs is associated with $[Fe(II)–OH_2]$ and [Fe(III)–OH] moieties, respectively. By analogy, the characterisation of pairs of $[Mn(II)–OH_2]$ and [Mn(III)–OH] which are related by an H$^\bullet$, is of interest for Mn–LOX modelling. While aqua complexes for Mn(II) are well known, examples of the Mn(III)–hydroxide motif are few, no doubt due to their reactivity.[9,10]

We describe here labile Mn complexes of the mononegative pentadentate N_4O ligands, *N*-glycyl-*N′*-methyl-*N*,*N′*-bis(2-pyridylmethyl)-1,2-ethanediamine (mgbpen$^-$) and *N*-benzyl-*N′*-glycyl-*N*,*N′*-bis(2-pyridylmethyl)-1,2-ethanediamine (bzgbpen$^-$), generic abbreviation, Rgbpen, R = CH_3, $CH_2C_6H_5$, Chart 1. A very accurate [Fe(III)–OH] model for the active Fe-lipoxygenases (Fe–LOXs) can be generated using this system.[11] By carrying out the parallel Mn chemistry we have identified a [Mn(III)–OH], Mn–LOX relevant species. Further-

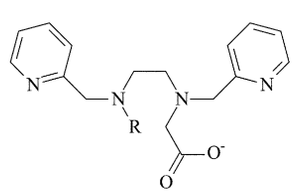

mgbpen$^-$, R=CH_3
bzgbpen$^-$, R=$CH_2C_6H_5$

Chart 1

† Electronic supplementary information (ESI) available: The ESI mass spectra of **1** at various tube-lens potentials. See http://www.rsc.org/suppdata/dt/b3/b300823a/

DOI: 10.1039/b300823a

more, the ligands show a relatively large degree of flexibility since dinuclear species for II–II, III–III, III–IV, IV–IV oxidations states have been identified. These differ in their Mn ligation and geometry and may be relevant to OEC modeling, since the carboxylate groups can switch from bridging ligation in Mn(II)–Mn(II) complexes to terminal ligation, concomitant with formation of one or two oxo bridges in Mn(III)–Mn(III) and Mn(IV)–Mn(IV) complexes, respectively. These limiting structures represent a "carboxylate shift". Such shifts are presumed crucial for controlling O_2 activation reactions in the non-heme diiron proteins.

Results and discussion

Mn(II) complexes

The reaction of mgbpenH and bzgbpenH with Mn(II) perchlorate in an aqueous solution open to the atmosphere gives $[Mn_2(mgbpen)_2(H_2O)_2](ClO_4)_2$ (**1**) and $[Mn_2(bzgbpen)_2(H_2O)_2](ClO_4)_2$ (**2**), respectively. The complexes are air stable in solution and solid state. Crystal structure analysis shows that **1** is dinuclear with (μ-κ*O*)-bridging by one oxygen atom of the $mgbpen^-$ carboxylate group, Fig. 1. The Mn atoms are seven-coordinated by five donor atoms from one ligand, a carboxylate oxygen atom from the ligand bound to the adjacent manganese ion, and a water molecule. The bridging Mn–O2 distances are significantly different at 2.2313(16) and 2.5908(16) Å. The Mn ··· Mn distance is 4.0914(9) Å. One hydrogen atom (H17A) of the water ligand on each manganese ion is strongly H-bonded to the non-coordinated carboxylate oxygen atom of $mgbpen^-$ on the adjacent manganese ion, O1 ··· O3, 2.583, O1–H 0.835 and O3 ··· H 1.779 Å. We have no crystal structure for **2**, however the similarity in IR, CV and ESI MS data for **1** and **2** is the basis for assigning analogous dimeric structures. The arrangement of the H-bonded carboxylate and water ligands at the dimanganese site represents an arrangement which may be a relevant limiting form for the carboxylate shift mechanism. The structure of the reduced Mn(II)–Mn(II) centre in Mn-substituted ribonucleotide reductase R2 protein shows a terminal water on one Mn(II) and a monodentate aspartate on the other,[3] however inspection of this protein structure does not indicate an interaction as close as that observed for **1**.

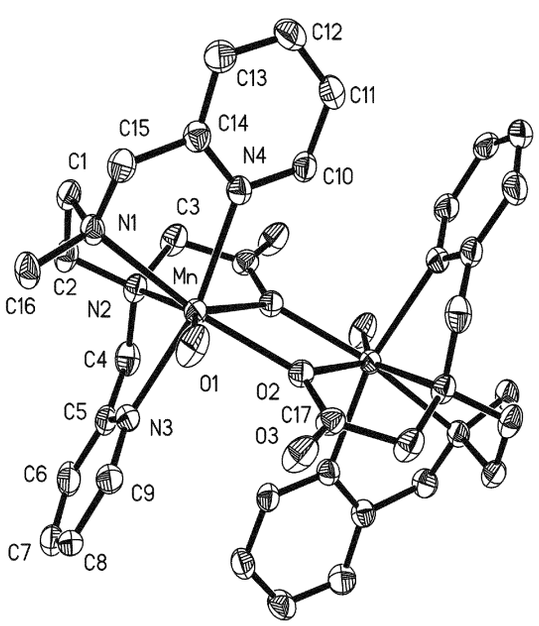

Fig. 1 X-Ray crystal structure of $[Mn_2(mgbpen)_2(H_2O)_2](ClO_4)_2$ (**1**). Important distances (Å): Mn–O1 2.204(2), Mn–O2 2.2313(16), Mn–N4 2.246(2), Mn–N3 2.290(2), Mn–N2 2.329(2), Mn–N1 2.419(2), Mn–O2#1 2.5908(16).

Dimers for the dehydrated ions derived from **1** and **2** are observed in ESI mass spectra. The doubly-charged peaks at *m/z* 368.1 and at *m/z* 444.4 are assigned $[Mn_2(mgbpen)_2]^{2+}$ and $[Mn_2(bzgbpen)_2]^{2+}$, respectively. As the source conditions are made increasingly harsh, monomeric singly-charged ions with the same *m/z* values, $[Mn(Rgbpen)]^+$ grow in. When the tube lens is above 80 V the peak is 100% composed of $[Mn(Rgbpen)]^+$ (see ESI †).

Magnetic properties and EPR spectra of 1

The magnetic susceptibility of **1** has been investigated in the temperature range 5–300 K at 0.5 and 5 T. Fig. 2 illustrates the temperature dependence of the product of the molar magnetic susceptibility (χ_m) and temperature. The room-temperature value of $\chi_m T$ is 8.6 cm^3 K mol^{-1} close to that expected for two non-interacting spins $S = 5/2$. When T decreases, $\chi_m T$ decreases smoothly until 50 K where it reaches 6.8 cm^3 K mol^{-1}, and then more abruptly to 1.3 cm^3 K mol^{-1} at 5 K. Such a behavior is characteristic of a pair of weakly antiferromagnetically coupled manganese(II) ions. It is noteworthy that the χ_m *vs.* T curve exhibits a maximum at *ca.* 9 K (data not shown). The experimental data could be accounted for by using the van Vleck equation for two interacting spins $S = 5/2$ (see Experimental section). The solid line in Fig. 2 represents the best fit obtained with the following parameters: $g = 2$, $-J = 1.3(1)$ cm^{-1} and TIP = $3(1) \times 10^{-4}$ cm^3 mol^{-1}.

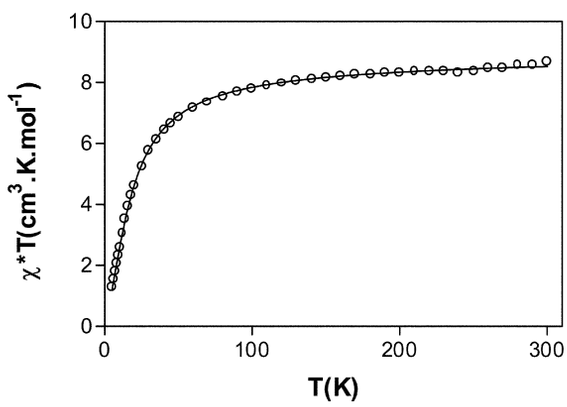

Fig. 2 Temperature dependence of the $\chi_m T$ product of **1**. Data collected at 0.5 T. The solid line corresponds to the fit obtained with the following parameters: $g = 2$, $-J = 1.27$ cm^{-1}, TIP = 3×10^{-4} cm^3 mol^{-1}.

The X-band EPR spectrum of powdered samples of **1** is broad. It shows similar features but becomes more resolved in a MeOH–DMF solution, Fig. 3. Centered around $g = 2$ is a broad band with more than 25 hyperfine splittings of *ca.* 45 G suggesting that **1** retains its dimeric structure in solution. Additional broad features both at high field $g = 1.6$ and at low field $g = 3.26$

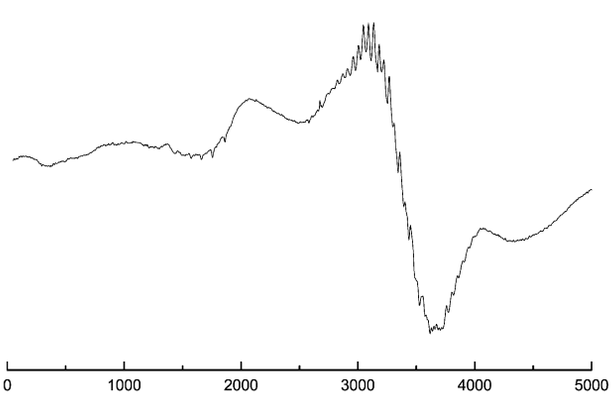

Fig. 3 The EPR spectrum of **1** in frozen-glass MeOH–DMF solution, 105 K.

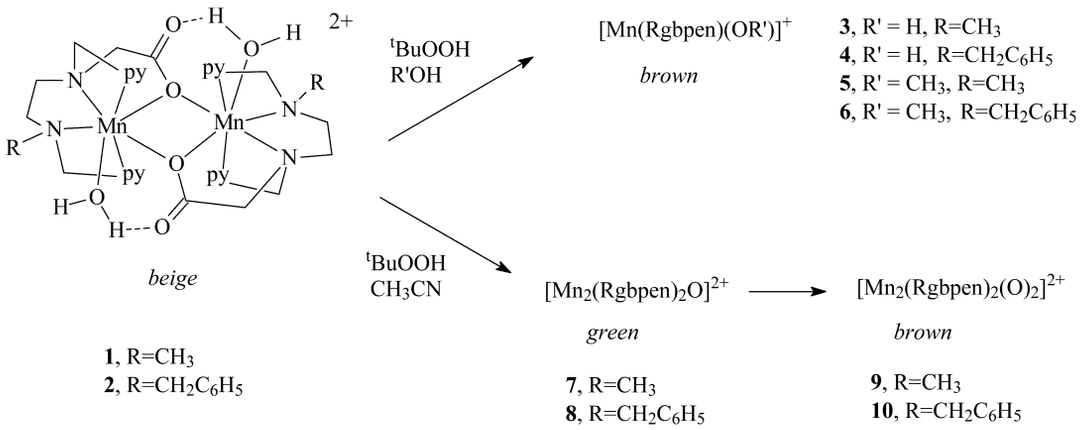

Scheme 1

and g = 6.26 are observed. The EPR spectrum of **1** bears a strong resemblance to that for the dimanganese(II) complex $Mn_2(H_2O)(OAc)_4(tmeda)_2$ (tmeda = *N*,*N*,*N*′,*N*′-tetramethylenediamine) which was recently the subject of a detailed X- and Q-band EPR study. Indeed, analogous transitions are observed but they maximize at different temperatures owing to the smaller antiferromagnetic coupling in **1** (−1.3 *vs* −2.9 cm^{-1}).[12]

Solvent dependent oxidation of 1 and 2

The seven coordination of the manganese atoms in **1** and **2** most likely protect the complexes from spontaneous air oxidation in the solid state and solution. This might otherwise have been expected for Mn(II) complexes of ligand systems comprising carboxylate, pyridine and amine donor atoms. The formation of bubbles upon addition of dihydrogen peroxide to **1** in acetonitrile (and concomitant color change to pale yellow) and in methanol (no color change) suggests that the Mn(II) complexes show catalase activity. However by using *tert*-butyl hydroperoxide (TBHP) we could generate higher oxidation state species from **1** and **2**. Unstable (hours–days) brown solutions develop on the addition of TBHP to the complexes in hydroxylic solvents. Usually a transient (seconds) green coloration formed before the brown color. After *ca.* half a day in hydroxylic solvent, and several days in acetonitrile the solutions bleached and the starting complexes could be detected by ESI-MS. We have characterized the brown and green species in acetonitrile solution and the brown only in hydroxylic solvents. Scheme 1 presents a summary of the reactions and the assignments proposed on the basis of the UV-visible, EPR spectroscopy, ESI MS and cyclic voltammetry experiments. The mononuclear $[Mn(III)(mgbpen)(OH)]^+$ and $[Mn(III)(bzgbpen)(OH)]^+$ species, **3** and **4**, respectively, and $[Mn(III)(mgbpen)(OCH_3)]^+$ and $[Mn(III)(bzgbpen)(OCH_3)]^+$, species **5** and **6**, respectively, are generated from complexes **1** and **2** in water or methanol, respectively. By contrast, the longer lived bis-μ-oxo-dimanganese(IV) complexes (**9** and **10**) are generated in acetonitrile *via* shorter lived oxo-bridged dimanganese(III) compounds (**7** and **8**).

Reactions of **1** or **2** with two equivalents of TBHP in water or methanol give brown EPR silent solutions with a lifetime of several hours at room temperature. The UV-visible spectrum for the oxidation of **1** in water recorded over 1 h is shown in Fig. 4. The final spectrum of the brown solution, after 48 min and a total of 10 eq. TBHP, shows bands at 420 nm (sh, 1714 M^{-1} cm^{-1}), 548 nm (sh, 462 M^{-1} cm^{-1}) and 650 nm (335 M^{-1} cm^{-1}). The initial green solution obtained after just 3 min reaction with 2 eq. TBHP, has a band at 427 nm (315 M^{-1} cm^{-1}) and at 559 nm (155 M^{-1} cm^{-1}). Due to its short lifetime we have not obtained other spectroscopic data for the initial green species. Over *ca.* 12 h the brown color bleaches. The ESI mass spectra of the brown solutions contain ions at *m*/*z* 385.2 (expected *m*/*z* 385.3) and 399.1 (expected *m*/*z* 399.5 (see ESI †))

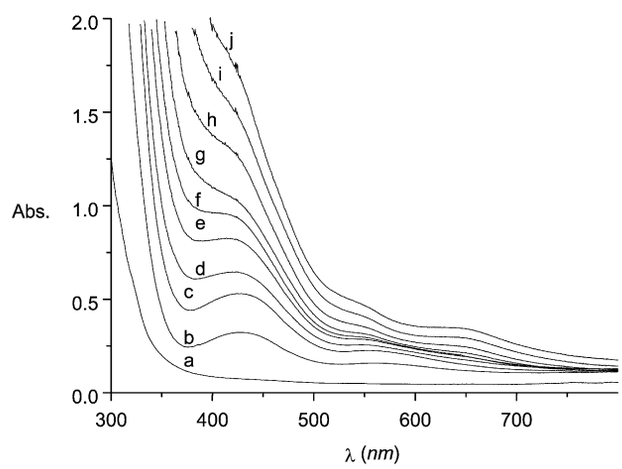

Fig. 4 Time resolved UV-visible spectra of the oxidation of **1** in water by 2 eq. TBHP (a–f), and at t = 33 min addition of another 8 eq. TBHP (g–j). (a): 0 min, (b): 3 min, (c): 6 min, (d): 9 min, (e): 15 min, (f): 30 min, (g): 36 min, (h): 42 min, (i): 45 min, (j): 48 min.

corresponding to the singly-charged **3** (Fig. 5(b)) and **5**. Variation of the tube lens potentials shows that the $[Mn(III)(Rgbpen)(OH)]^+$ ions are solution-derived. Alternative sources for these ions can be discounted. They are not derived from $[Mn^{II}(Rgbpen)(OHR')]^+$, R′ =H, CH_3, ions by loss of an H atom or methyl radical, since aqua and methanol complexes will preferentially lose the neutral solvent ligand under all but very mild source conditions. The ESI mass spectrum of the Mn(II) complexes **1** and **2** demonstrate this phenomenon: no traces of the oxidised species **3**, **4**, **5** and **6** were observed. Addition of D_2O to the aqueous solution of **4** results in a new signal in the ESI mass spectrum 1 mass unit above the singly charged **4** corresponding to $[Mn(III)(bzgbpen)(OD)]^+$.

The color changes when the TBHP oxidation of **1** and **2** is carried out in acetonitrile are similar to those in methanol, however the chromophores are due to different products. When 2 eq. TBHP react with **1** and **2** a transient green colour ($t_{½}$ < 1 s for the mgbpen$^-$ system and seconds to minutes for the bzbpen$^-$ system) and a final unstable brown color also appears in the EPR silent solutions at room temperature. By complementary and parallel use of ESI MS, CV, UV-visible and EPR spectroscopy, we have characterized both the transient green and brown oxidized species formed in these reactions. The reaction followed by UV-visible spectroscopy is shown in Fig. 6. The green compound **7** achieves its maximum concentration after reacton of **1** with 2 eq. of TBHP for 3 min; 430 nm (sh, 825 M^{-1} cm^{-1}), 561 nm (300 M^{-1} cm^{-1}) (Fig. 6(A) spectrum (b)). In spectrum (h), the brown compound **9** is at maximum concentration after 39 min; 528 nm (sh, 655 M^{-1} cm^{-1}) and 645 nm (390 M^{-1} cm^{-1}). Correspondingly in Fig. 6(B), spectrum (e), shows **8** in maximum concentration after 59 min; 435 nm (sh,

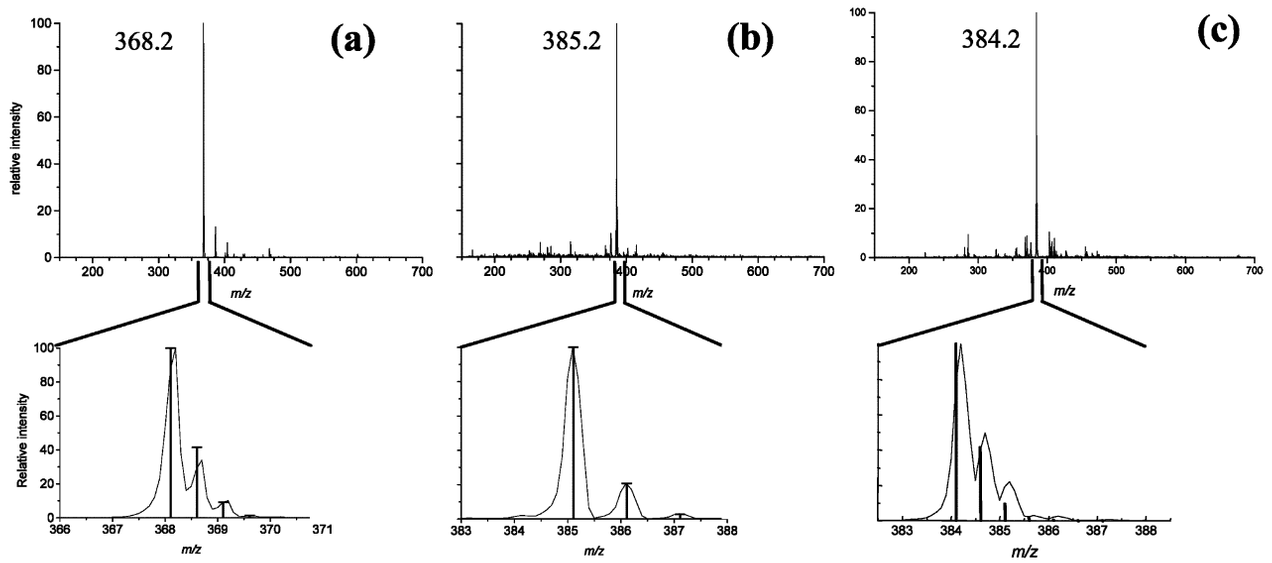

Fig. 5 The ESI mass spectrum of (a) an acetonitrile solution of **1**, *m*/*z* 368.2 = $[Mn_2(mgbpen)_2]^{2+}$; (b) a water solution of **1** after reaction with ^{t}BuOOH, *m*/*z* 385.2 $[Mn(OH)(mgbpen)]^+$ (**3**); (c) an acetonitrile solution of **1** after reaction with ^{t}BuOOH, *m*/*z* 384.2 = $[Mn_2O_2(mgbpen)_2]^{2+}$ (**9**). Peak expansions and calculated isotopic fits below.

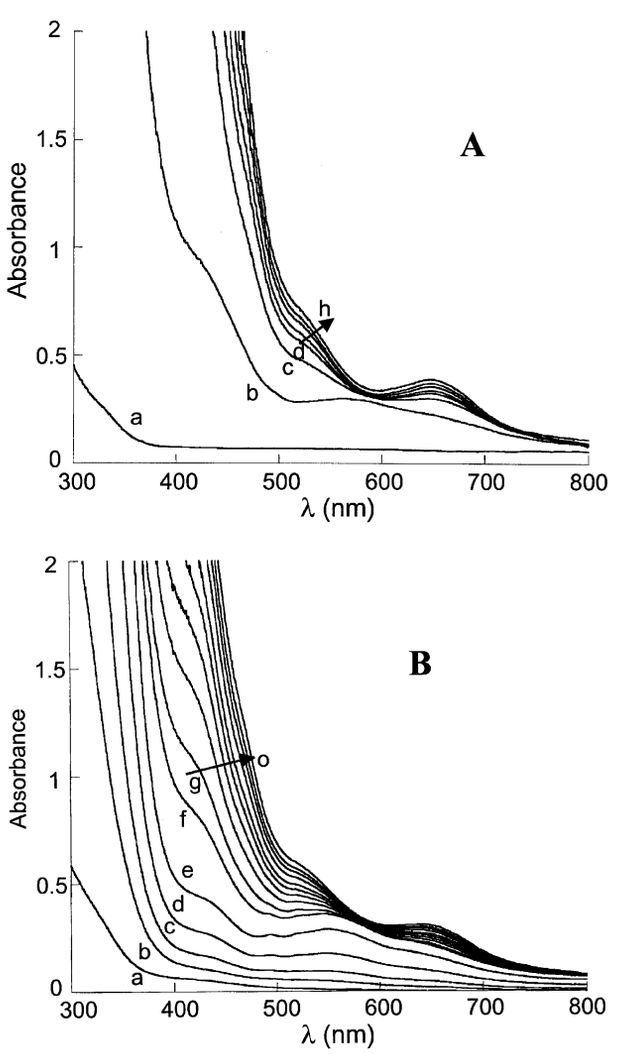

Fig. 6 Time resolved UV-visible spectra after addition of 2 equivalents of TBHP in (A) a 1.07 mM solution of **1** in CH_3CN, 0.1 M Bu_4NClO_4: (a) initial solution; (b) after 3 min; (c) 6 min; (d) 9 min; (e) 12 min; (f) 18 min; (g) 24 min; (h) 39 min; l = 1 cm. (B) 1.05 mM solution of **2** in CH_3CN, 0.1 M Bu_4NClO_4: (a) initial solution; (b) after 44 min; (c) 49 min; (d) 54 min; (e) 59 min; (f) 1 h 02 min; (g) 1 h 05 min; (h) 1 h 11 min; (i) 1 h 17 min; (j) 1 h 23 min; (k) 1 h 28 min; (l) 1 h 38 min; (m) 1 h 48 min; (n) 1 h 58 min; (o) 2 h 23 min; l = 1 cm.

410 M^{-1} cm^{-1}), 495 nm (260 M^{-1} cm^{-1}), 520 nm (270 M^{-1} cm^{-1}), 550 nm (290 M^{-1} cm^{-1}), 650 (sh, 165 M^{-1} cm^{-1}) and compound **10** at maximum concentration after 2 h 23 min (spectrum (o)); 524 nm (sh, 540 M^{-1} cm^{-1}), 645 nm (300 M^{-1} cm^{-1}).

The green and brown species are detected by ESI MS: the doubly-charged ions for the more stable brown dioxo compounds being most easily observed. Fig. 5(c) shows **9** (*m*/*z* 384.2) at one mass unit lower than that for the singly-charged **3** in the mass spectrum. As shown by UV-visible spectroscopy the reaction times are slower for the benzyl substituted system and for this system we were able to trap the ions associated with the green species. The spectrum in Fig. 7 is very clean and shows only ions assigned to $[Mn(bzgbpen)]^+$ (*m*/*z* 444.1, dehydrated monomer from **2**), $[(Mn(bzgbpen))_2O]^{2+}$ (**8**, *m*/*z* 452.1) and $[(Mn(bzgbpen))_2O_2]^{2+}$ (**10**, *m*/*z* 460.1). A second ion overlaps with *m*/*z* 460.1; this can be assigned to $[(bzgbpen)Mn(OH)]^+$ (**4**) at *m*/*z* 461.1. A simulation of the isotope pattern indicates a 29% : 71% composition of the signals from **4** and **10**. The presence of small amounts of **4** in the acetonitrile reactions is probably due to traces of water. Over a period of minutes to hours the intensity of the signal corresponding to **2** decreases while those for **8** and **10** increase. After many hours the inten-

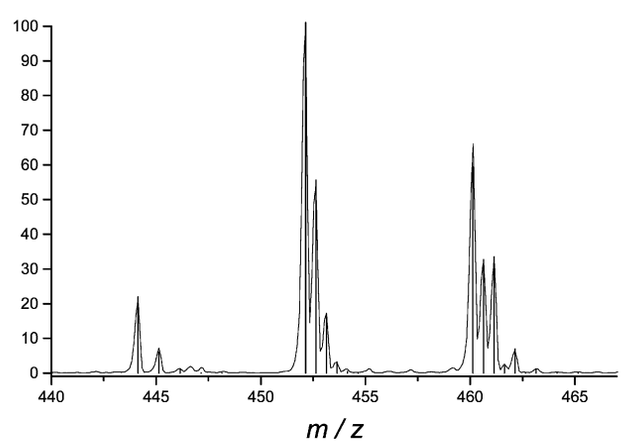

Fig. 7 ESI-MS of **2** in acetonitrile after reaction with one equivalent of TBHP. Recorded after 6 min. The calculated isotopic fits are depicted as bars. Assignments: *m*/*z* 444.1, $[Mn(bzgbpen)]^+$; *m*/*z* 452.1, $[(Mn(bzgbpen))_2O]^{2+}$ (**8**); 460.1, $[(Mn(bzgbpen))_2O_2]^{2+}$ (**10**). The 460.1 contains a second ion, $[(bzgbpen)Mn(OH)]^+$ (**4**) at *m*/*z* 461.1. A simulation indicates a composition of 29% **4** and 71% **10**.

sity of **10** starts to decrease while **2** grows in and **8** remains fairly constant. After 2 days only the starting material, **2**, is present. The rate of reaction is faster for the oxidation of **1**. The ESI mass spectrum of a brown solution obtained by addition of 2 equivalents of TBHP and recorded after 6 min presents the doubly-charged ion at *m*/*z* 384.2 due to **9** (Fig. 5(c)) with no trace of **7** evident.

The oxidation processes in acetonitrile followed by cyclic voltammetry (CV) are shown in Figs. 8 and 9. As for the ESI MS results a clean separation of the species was observed and the assignments fully corroborate those made by ESI MS. Similar to a known manganese(II) dimer doubly-bridged by one oxygen atom of carboxylate groups,[13] CVs of **1** and **2** in CH_3CN show irreversible oxidation waves at $E_{pa} = 0.90$ and 1.23 V *vs.* Ag/Ag^+ 10^{-2} M (Fig. 8(A)) and $E_{pa} = 0.92$ and 1.24 V (Fig. 9(A)), respectively. These waves progressively disappear after addition of two equivalents of TBHP in solutions while new waves corresponding to the formation of transient green solutions of **7** and **8** and brown solutions of **9** and **10** appear. The formation of **8** can be clearly observed after 1 h 02 min by the appearance of two successive reversible one-electron oxidation waves at $E_{1/2} = 0.70$ V ($\Delta E_p = 80$ mV) and $E_{1/2} = 1.21$ V ($\Delta E_p = 90$ mV) and an irreversible one-electron reduction peak at $E_{pc} = -0.26$ V (Fig. 9(C)). For **7**, after 5 min, these redox systems are located at $E_{1/2} = 0.68$ V ($\Delta E_p = 80$ mV), $E_{1/2} = 1.17$ V ($\Delta E_p = 90$ mV) and $E_{pc} = -0.13$ V (Fig. 8(B) while additional small reduction peaks at $E_{pc} = 0.26$ V and $E_{pc} = -0.45$ V correspond to the concomitant formation of some amount of **9**. The shape of these CVs of **7** and **8** are very similar to that obtained for the most closely related mono-oxo bridged $Mn(III)_2$ complex with pentadentate phenolate ligands.[14] Thus the two oxidation waves can be assigned to the $Mn(III,III)_2/Mn(III,IV)_2$ and $Mn(III,IV)_2/Mn(IV,IV)_2$ redox couples, and the reduction peak to the $Mn(III,III)_2/Mn(III,II)_2$ couple.

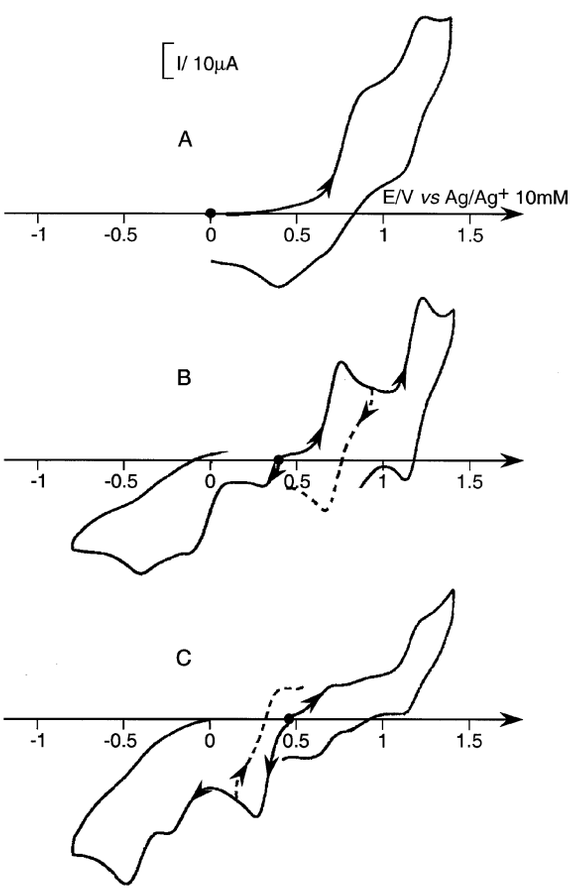

Fig. 8 Time resolved cyclic voltammograms at a platinum electrode in CH_3CN of the reaction of **1** with TBHP to form the green **7** and brown **9**, of (A) 1.07 mM of **1**; (B, C) after addition of 2 equivalents of ^{t}BuOOH: (B) after 5 min (CV due predominantly to **7**), (C) after 40 min (CV due predominantly to **9**). 0.1 M Bu_4NClO_4, sweep rate 100 mV s^{-1}.

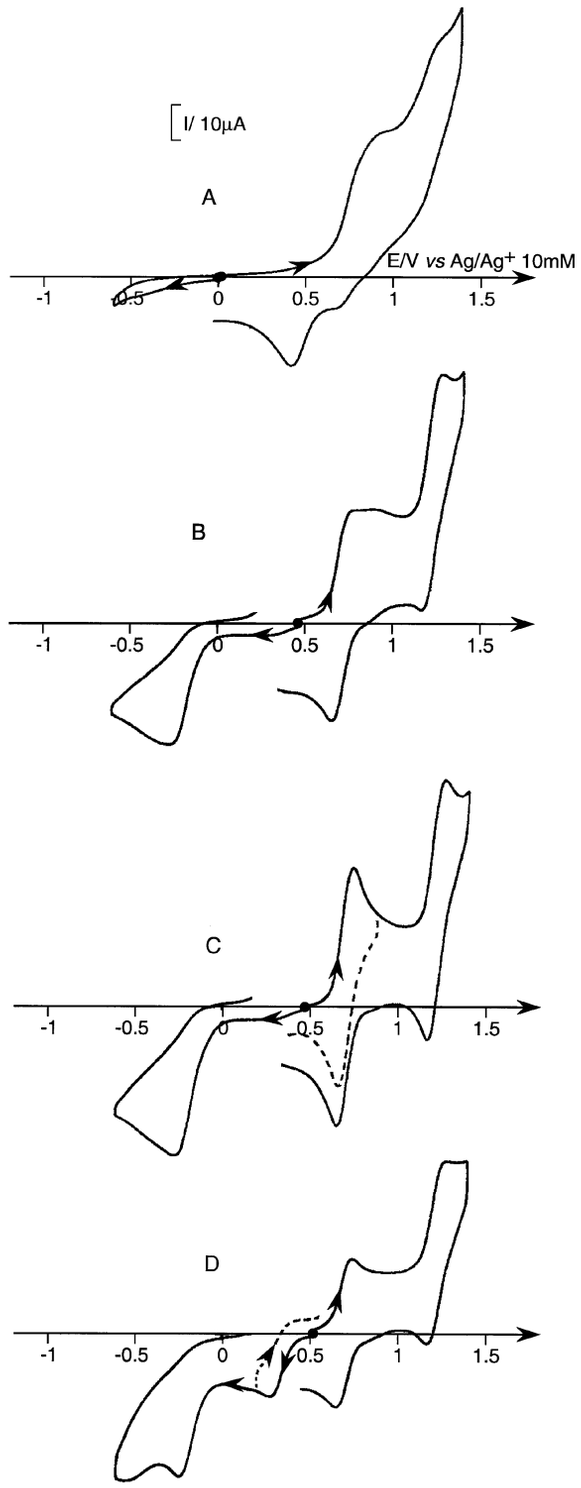

Fig. 9 Time resolved cyclic voltammograms at a platinum electrode in CH_3CN of the reaction of **2** with TBHP to form the green **8** and brown **10**. (A) 1.05 mM of **2**; (B–D) after addition of 2 equivalents of ^{t}BuOOH: 55 min (B), 1 h 02 min (C), 2 h 23 min (D). The transient green intermediate **8** in more dominant in (B–D) compared to the corresponding results in Fig. 8. 0.1 M Bu_4NClO_4, sweep rate 100 mV s^{-1}.

After a few minutes in the case of **1** (or a few hours for **2**), the formation of the higher oxidation state di-oxo-dimanganese(IV) complexes **9** (or **10**) can be observed by the appearance of a poorly reversible one-electron reduction wave at $E_{pc} = 0.26$ V followed by an irreversible one at $E_{pc} = -0.48$ V (Fig. 8(C)). These values are similar to those of the most closely related di-μ-oxo dimanganese(IV) complex in the literature [13] and corre-

spond to the $Mn(IV,IV)_2/Mn(III,IV)_2$ and $Mn(III,IV)_2/Mn(III,III)_2$ redox couples. In the case of **9**, and unlike the majority of the di-μ-oxo dimanganese compounds having bi- or tetra-dentate ligands, the $Mn(IV,IV)_2/Mn(III,IV)_2$ wave is only poorly reversible showing the instability of the mixed-valent $[Mn_2(mgbpen)_2O_2]^+$ species. The presence of a shoulder at $E_{pc} = -0.25$ V preceeding the irreversible reduction at $E_{pc} = -0.48$ V (Fig. 8(C)) is also observed resulting probably to the presence of a small amount of **7** remaining in solution and to the poor stability of the first $Mn(III,IV)_2$ reduced species formed on the time scale of the CV. It is clear from with the two reduction waves located at E_{pc} = 0.27 V and $E_{pc} = -0.53$ V that **10** and **9** have similar electrochemistry. However, **10** cannot be quantitatively formed, and an equilibrium is reached after about 2 h 30 min (Fig. 9(D)). In summary, the electrochemical results corroborate UV-visible spectroscopy and ESI MS in showing that the rate of formation of oxidised complexes is faster for **1** compared to **2**. In the case of **1**, the almost quantitative formation of **9** takes about 40 min (Fig. 8(C)) while for **2**, only 50% of **10** can be reached after 2 h 30 min. Moreover, in the case of **1**, although the rate of formation of **9** is slower than that of **7**, the two processes overlap and **7** cannot be exhaustively formed. A maximum concentration of **7** is obtained after 5 min, but at this time some compound **9** is already present (Fig. 8(B)). In the case of **2**, **8** can be quantitatively obtained after about 1 h (Fig. 9(C)) while **10** cannot be quantitatively formed (Fig. 9(D)). By recording the CV in parallel with the UV-visible spectra, and by taking advantage of the differences in the rates of formation, we were able to identify the redox waves associated with the transient green Mn(III)–(μ-O)–Mn(III) species and brown Mn(IV)–$(\mu\text{-O})_2$–Mn(IV) species for the $mgbpen^-$ derivative **8** and $bzbpen^-$ derivative **9**, respectively.

Clearly conclusions cannot be drawn from the EPR silence observed for the UV-visible spectroscopically, mass spectrometrically and electrochemically different brown chromophores in hydroxylic solvent (**3**, **4**, **5**, **6**) and acetonitrile (**9**, **10**) and the even shorter-lived green chomophores (**7**, **8**) in acetonitrile. However it is consistent with (i) the complete disappearance of **1** and **2** and (ii) the $[Mn^{III}(Rgbpen)(OR')]^+$, R′=H, CH_3, $[Mn_2^{III}(Rgbpen)_2(O)]^{2+}$, and $[Mn_2O_2(Rgbpen)_2]^{2+}$ assignments for different reasons: d^4 configuration in the two first cases and strongly antiferromagnetically coupled d^3–d^3 in the last case.

Conclusions

The dimeric nature of **1** and **2** bears little structural relevance to the putative mononuclear reduced Mn(II)–OH_2 site in reduced Mn–LOX. However it does imply one important point: seven coordination of the metal ion might inhibit its oxidation and this may be a useful activation/de-activation switch mechanism for the Mn(II) state of Mn–LOX and other manganese-containing enzymes. Six coordination (five amino acid donors and one water) is established by X-ray crystallography for Fe^{II}–LOX. A difference in the metal binding sites in Mn–LOX from Fe–LOXs is clear from the difference in the α helix 9 sequence containing the two His metal donors: there are 30 members in Fe LOX and 28 members Mn–LOX. Oliw and co-workers suggest that this is probably of paramount importance for the geometry at the metal centre, the metal ion specificity and enzyme activity.[8] Using the dimeric complexes **1** and **2**, the UV-visible, EPR, MS, and electrochemical characterisation of active Mn–LOX $[Mn(III)–OH]^+$ models generated by a biomimetic alkylperoxide oxidation has been achieved. These species do not have the EPR and Mössbauer spectroscopic handles available in the study of analogous iron species. Since the donor set to Mn(III) in **3**, **4**, **5** and **7** is similar to that predicted for oxidized Mn–LOX future comparison of the spectroscopic characteristics reported herein may be useful in analysis of the enzyme.

The outcome of alkylperoxide oxidation is solvent controlled. The detection of oxo-bridged $Mn(III)_2$ and $Mn(IV)_2$ dimers in acetonitrile suggests to us that the more unusual Mn(III)–OH species characterized in hydroxylic solvent, is stabilized by hydrogen bonding to the solvent. It is likely that if the mononuclear Mn(III)–OH species are produced in acetonitrile a rapid dimerisation by dehydration occurs to give the green Mn(III) oxo-bridged dimers, **7** and **8**. This species is then susceptible to further oxidation by either TBHP or O_2 to give the brown species **9** and **10**.

The series of Mn dimers from Mn(II)Mn(II) to Mn(IV)Mn(IV) oxidation states is particularly interesting with respect to the relevance of the system to OEC and number of dimeric species accessible. Using several techniques it can be argued that six oxidation states (II–II, II–III, III–III, III–IV, IV–IV, IV–V) are accessible using these new mononegatively-charged pentadentate ligands (mixed valence species implicated by electrochemistry only). The structure of **1** shows a H-bonding arrangement for water and non-coordinated oxygen of Asp or Glu on adjacent metal ions around 4 Å apart. Of particular importance is the inclusion of a carboxylate in the ligand system and the interplay of the carboxylate shift mechanism and formation of oxo bridges.

Experimental

^1H and ^{13}C NMR spectra were recorded on a 300 MHz Varian Gemeni 2000 spectrometer using tetramethylsilane (TMS) as an internal reference; *J* values are given in Hz. Elemental analysis were performed at the Chemistry Department II at Copenhagen University, Denmark and Atlantic Microlab, Inc., Norcross, Georgia 30091, USA. UV-visible spectra were recorded on a Shimadzu UV-3100 spectrophotometer and on Varian Cary 50 Probe and Cary 100 Scan spectrometers. IR spectra of the complexes in KBr discs were measured using a Hitachi 270–30 IR spectrometer. Electrospray ionization mass spectra (ESI MS) were obtained using a Finnigan TSQ 700 triple quadrupole instrument equipped with a Finnigan API source in the nanoelectrospray mode (Protana, Denmark). Electron paramagnetic resonance (EPR) measurements at X-band frequency were obtained using a Bruker ESP-380E FT-EPR spectrometer. TBHP 5–6 M in decane was used for the oxidation reactions.

CAUTION: Perchlorate salts of metal complexes with organic ligands are potentially explosive. Only small quantities of the compounds should be prepared and handled behind suitable protective shields.

Ligand syntheses

***N*,*N*′-Bis(2-pyridylmethyl)imidazolidine.** *N*,*N*′-Bis(2-pyridylmethyl)-1,2-diaminoethane (7.0 g, 29 mmol) and paraformaldehyde (0.86 g, 29 mmol) were refluxed in diethyl ether (120 ml) with 4 Å molecular sieves overnight with $CaCl_2$ protection. After filtration the solution was evaporated *in vacuo* to yield a dark yellow oil (5.8 g, 79%). δ_H ($CDCl_3$): 2.96 (4H, s, NCH_2CH_2N), 3.61 (2H, s, NCH_2N), 3.92 (4H, s, 2 × $NCH_2C_5H_4N$), 7.17 (2H, t, *J* 5.98, 2 × C^4H py), 7.48 (2H, d, *J* 7.70, 2 × C^3H py), 7.67 (2H, t, *J* 6.31, 2 × C^5H py), 8.55 (2H, d, *J* 4.12, 2 × C^6H py). δ_C ($CDCl_3$): 52.6 (NCH_2CH_2N), 61.2 (2 × $NCH_2C_5H_4N$), 76.8 (NCH_2N), 122.0, 122.7 (2 × C^3 py, 2 × C^5 py), 136.5 (2 × C^4 py), 149.1 (2 × C^6 py), 159.3 (2 × C^2 py).

***N*-Methyl-*N*,*N*′-bis(2-pyridylmethyl)-1,2-ethanediamine (another synthesis has been reported[15]).** $NaBH_3CN$ (3.23 g, 51.4 mmol) was added to a stirred solution of *N*,*N*′-bis(2-pyridylmethyl)imidazolidine (5.4 g, 21.2 mmol) in dry methanol (80 ml). CF_3COOH (11.70 g, 102 mmol) was added and the solution was stirred overnight with $CaCl_2$ protection. 15% aqueous sodium hydroxide (65 ml) was added and the solution was stirred for another 6 h. The resulting solution was extracted

with CH_2Cl_2 (3 × 20 ml), dried on Na_2SO_4 and evaporated *in vacuo* to yield a brown oil (4.5 g, 83%). δ_H ($CDCl_3$): 2.07 (3 H, s, NCH_3), 2.46 (2 H, m, $NCH_2CH'_2N$), 2.59 (2 H, m, $NCH_2CH'_2N$), 3.48 and 3.72 (2 H, s, and 2 H, s, 2 × $NCH_2C_5H_4N$), 6.96–7.46 (6 H, m, 2 × C^4H, C^5H and C^6H py) 8.35 (2 H, m, 2 × C^3H py). δ_C ($CDCl_3$): 42.63 (NCH_3), 46.80 ($CH_2NHCH_2C_5H_4N$), 55.31 ($NHCH_2C_5H_4N$), 57.29 ($C_5H_4NCH_2(CH_3)NCH_2$), 64.13 ($C_5H_4NCH_2NCH_3$), 121.89, 121.98, 122.25, 123.11 (2 × C^3 py, 2 × C^5 py), 136.43, 136.46 (2 × C^4 py), 149.04, 149.31 (2 × C^6 py), 159.56, 160.07 (2 × C^2 py).

***N*-Methyl-*N′*-glycine-*N*,*N′*-bis(2-pyridylmethyl)-1,2-ethanediamine (mgbpenH).** Bromoacetic acid (2.45 g, 17.6 mmol) and triethylamine (1.79 g, 17.7 mmol) were added to a solution of *N*-methyl-*N*,*N′*-bis(2-pyridylmethyl)-1,2-ethanediamine (4.50 g, 17.6 mmol) in dry ethanol (2 ml). The solution was refluxed under N_2 for 24 h and then evaporated under vacuum. The oily residue was dissolved in water (10 ml) and pH was adjusted to 10 with conc. aqueous NaOH. The dark solution was extracted with CH_2Cl_2 (3 × 10 ml) and the aqueous phase was evaporated *in vacuo* to yield a brown oil (5.48 g, 93%). δ_C ($CDCl_3$): 40.80 (NCH_3), 49.52 ($CH_2N(CH_2C_5H_4N)(CH_2COO^-)$), 53.81 ($(CH_3)(CH_2C_5H_4N)NCH_2$), 58.22 ($(CH_2COO^-)N(CH_2C_5H_4N)$), 59.72 ($C_5H_4NCH_2NCH_3$), 60.00 ($NCH_2COO^-$), 123.41, 124.28, 124.84, 125.58 (2 × C^3 py, 2 × C^5 py), 138.51, 138.66 (2 × C^4 py), 148.26, 149.50 (2 × C^6 py), 156.55 (C^2 py).

2-Phenyl-1,3-bis(2-pyridylmethyl)imidazolidine. *N*,*N′*-Bis(2-pyridylmethyl)-1,2-ethanediamine (2.1 g, 10 mmol) and benzaldehyde (1.1 g, 10 mmol) were dissolved in 40 ml dry diethyl ether. The reaction was stirred with 4 Å molecular sieves overnight with $CaCl_2$ protection. The product was isolated as a white powder which was washed with dry ether (1.76 g, 57%). mp. 142–146 °C. δ_H ($CDCl_3$): 2.685, 3.305 (2 × 2H, m, NCH_2CH_2N (AA′BB′), 3.517 and 3.900 (2 H, d, *J* 14.12 and 2 H, d, *J* 13.88, 2 × $NCH_{AB}C_5H_4N$, A or B), 4.021 (1 H, s, $NCH(C_6H_5)N$), 7.081 (2 H, m, 2 × C^5H py), 7.2–7.45 (5 H, m, C_6H_5), 7.5–7.7 (4 H, m, C^3H py, C^4H py), 8.463 (2 H, d, C^6H py). δ_C ($CDCl_3$): 51.20 (NCH_2CH_2N), 58.82 (2 × $NCH_2C_5H_4N$), 89.00 ($NCH(C_6H_5)N$), 121.9, 122.9 (2 × C^5 py, 2 × C^3 py), 128.3 (C^3, C^5 Ph), 128.7 (C^4 Ph), 129.5 (C^2, C^6 Ph), 136.4 (2 × C^4 py), 140.1 (C^1 Ph), 148.8 (2 × C^6 py), 159.5 (2 × C^2 py).

***N*-Benzyl-*N*,*N′*-bis(2-pyridylmethyl)-1,2-ethanediamine.** 2-Phenyl-1,3-bis(2-pyridylmethyl)imidazolidine (1.5 g, 4.5 mmol) was dissolved in dry methanol (45 ml). The solution was filtered to remove molecular sieves from the previous step. $NaBH_3CN$ (0.28 g, 4.5 mmol) in 3 ml dry MeOH was added, and then CF_3COOH (1.0 g, 9.0 mmol) was added carefully. The reaction mixture was stirred for 24 h with $CaCl_2$ protection. 45 ml 15% aqueous NaOH was added and the reaction was allowed to stir for 6 h. This mixture was extracted with methylene chloride (20 ml) three times, the organic phase was dried on Na_2SO_4 and evaporated leaving a yellow oil (1.87 g, over 100% yield due to water and possible formation of sodium salt, however purity was sufficient for complex formation). δ_H ($CDCl_3$): 2.69 (1 H, br s, NH), 2.732 (4 H, m, NCH_2CH_2N), 3.637 (2 H, s, $NCH_2C_6H_5$), 3.751 (2 H, s, $NCH_2C_5H_4N$), 3.805 (2 H, s, $NCH_2C_5H_4N$), 7.0–7.2 (2 H, m, 2 × C^5H py), 7.2–7.45 (5 H, m, C_6H_5), 7.50–7.7 (4 H, m, 2 × C^3H py, 2 × C^4H py), 8.506 (2 H, m, 2 × C^6H py). δ_C ($CDCl_3$): 46.53, 53.60 (NCH_2CH_2N), 54.79 ($C_6H_5CH_2N$), 58.79, 60.21 (2 × $NCH_2C_5H_4N$), 121.65, 121.73, 121.95, 122.80 (2 × C^3 py, 2 × C^5 py), 126.82 (C^4 phen), 128.08 (C^3, C^5 phen), 128.78 (C^2, C^6, C^3, C^5 phen), 136.15, 136.24 (2 × C^4 py), 138.98 (C^1 phen), 148.64, 149.06 (2 × C^6 py), 159.77, 159.88, (2 × C^2 py).

***N′*-Benzyl-*N*-carboxymethyl-*N*,*N′*-bis(2-pyridylmethyl)-1,2-ethanediamine (bzgbpenH).** Bromoacetic acid (0.425 g, 3.05 mmol) and triethylamine (0.309 g 3.05 mmol) were added to a solution of *N*-benzyl-*N*,*N′*-bis(2-pyridylmethyl)-1,2-ethanediamine (1.014 g, 3.05 mmol) in dry ethanol (2.5 ml). The solution was refluxed overnight under N_2, put on ice to precipitate Et_3NHBr, which was removed. The solution was evaporated under vacuum and redissolved in water and adjusted to pH 8 with NaOH. The aqueous phase was washed three times with methylene chloride (3 × 15 ml) and adjusted to *ca.* pH 4 with aq. HCl. The solution was evaporated to an oil which was then redissolved in 15 ml absolute EtOH. Undissolved NaCl was removed and the solvent removed under vacuum to give a red–brown oil (0.799 g, 67%). δ_H (DMSO-d_6): 2.62–2.82 (4H, m, NCH_2CH_2N), 3.16 (2H, s, NCH_2COO^-), 3.4–3.8 (6H, m, 2 × $NCH_2C_5H_4N$ and $NCH_2C_6H_5$), 7.10–7.32 (7 H, m, C_6H_5 and 2 × C^5H py), 7.41 (2H, m, 2 × C^3H py), 7.67 (2H, m, 2 × C^4H py), 8.49 (2H, m, 2 × C^6H py). δ_C (DMSO-d_6): 51.3, 51.6 (NCH_2CH_2N), 57.7 ($NCH_2C_6H_5$), 59.3, 59.4 ($NCH_2C_5H_4N$), 60.1 (NCH_2COO^-), 121.5, 121.9, 122.4, 122.8 (2 × C^3 py, 2 × C^5 py), 126.7 (C^4 Ph), 128.1, 128.5 (C^2, C^6, C^3, C^5 Ph), 136.0, 136.4, (2 × C^4 Py), 138.9 (C^1 Ph), 148.5, 148.6 (2 × C^6 Py), 159.5, 160.6 (2 × C^2 Py), 173.4 (COOH).

Mn(II) complexes

$[Mn_2(mgbpen)_2(H_2O)_2](ClO_4)_2$ (1). $Mn(ClO_4)_2 \cdot 6H_2O$ (1.27 g, 3.5 mmol) in methanol (10 ml) was added to a solution of mgbpen (1.11 g, 3.3 mmol) in a 1 : 1 mixture of water–methanol (10 ml). After 3 days, the beige crystals were isolated by filtration. Yield 0.366 g (23%). ESI-MS (MeOH): *m*/*z* 368 (100%, $[(Mn(mgbpen))_2]^{2+}$). Anal. Calc. for $C_{34}H_{46}Cl_2Mn_2N_8O_{14}$: C, 42.03; H, 4.77; N, 11.53. Found: C, 41.64; H, 4.66; N, 11.25%. The synthesis of $[Mn_2(bzgbpen)_2(H_2O)_2](ClO_4)_2$ (**2**) is analogous. ESI-MS (MeCN): *m*/*z* 444.4 $[(Mn(bzgbpen))_2]^{2+}$, 987.4 $[\{(Mn(bzgbpen))_2\}(ClO_4)]^+$. Anal. Calc. for $C_{46}H_{54}Cl_2Mn_2N_8O_{14}$: C, 49.24; H, 4.85; N, 9.99. Found: C, 49.14; H, 4.38; N, 9.84%.

Magnetism. The magnetic susceptibility of compound $[Mn_2(mgbpen)_2(H_2O)_2](ClO_4)_2$ was measured over the temperature range 5–300 K at 0.5 and 5 T. The sample (25.6 mg) was contained in a kel F bucket which had been independently calibrated. The data were corrected from diamagnetism using Pascal's constants.[16] The data have been simulated using the van Vleck equation derived from the Heisenberg exchange hamiltonian ($H = -2JS_1 \cdot S_2$) for spins $S_1 = S_2 = 5/2$ (eqn. (1)): with $k = J/0.695T$ and t is the temperature independent paramagnetism. The *g* value was fixed to 2 in the calculations. The goodness of fit R^2 amounted to 0.9996.

Electrochemistry. Electrochemical measurements were performed using an EG&G PAR model 173 potentiostat/galvanostat equipped with a PAR model universal programmer and a PAR model 179 digital coulometer. The standard three-electrode electrochemical cell was used. In CH_3CN medium, the electrolyte was 0.1 M Bu_4NClO_4 and potentials were referred to an Ag/10 mM $AgNO_3$ reference electrode in CH_3CN, 0.1 M Bu_4NClO_4 electrolyte. Potentials referenced to that system can be converted to the SCE by adding 300 mV. The working electrode was a platinum disk (5 mm in diameter) polished with 2 μm diamond paste (Mecaprex Presi) for cyclic voltammetry (CV) (E_{pa}, anodic peak potential; E_{pc}, cathodic peak potential;

$$\chi_m T = 0.75g^2 \frac{\exp(2k) + 5\exp(6k) + 14\exp(12k) + 30\exp(20k) + 55\exp(30k)}{1 + 3\exp(2k) + 5\exp(6k) + 7\exp(12k) + 9\exp(20k) + 11\exp(30k)} + tT \quad (1)$$

$E_{1/2} = (E_{pa} + E_{pc})/2$; $\Delta E_p = E_{pa} - E_{pc}$). Exhaustive electrolyses were carried out with a 10 × 10 × 4 mm^3 carbon felt electrode (RCV 2000, 65 mg cm^{-3}, from Le Carbone Lorraine

X-Ray crystallography. Crystal data for $[Mn_2(mgbpen)_2(H_2O)_2](ClO_4)_2$ ($C_{34}H_{46}Cl_2Mn_2N_8O_{14}$): M_r = 971.57, yellow crystal (0.45 × 0.28 × 0.10 mm) from reaction mixture, triclinic, space group $P\bar{1}$, Z = 1, a = 8.3686(9), b = 9.8838(11), c = 13.1867(14) Å, α = 69.825(10), β = 85.749(10), γ = 78.412(10)°, V = 1002.92(19) Å^3, T = 120(2) K, D_c = 1.609 g cm^{-3}, $F(000)$ = 502, Mo-Kα radiation, λ = 0.71073 Å, μ = 0.840 mm^{-1}, transmission: 0.8635/0.9972. The intensities of 10572 reflections were measured on a Siemens/Bruker SMART 1K diffractometer. Data collection, integration of frame data and conversion to intensities corrected for Lorenz, polarization and absorption effects were performed using the programs SMART, SAINT[17] and SADABS[18] θ_{max} = 26.30°, 4106 independent reflections, R_{int} = 0.0207. Structure solution, refinement, structure analysis and production of crystallographic illustrations was carried out using the programs SHELXTL[19] and PLATON.[20] The refinement of 280 parameters (including H atom positions) with 4106 reflections converged at $R_1(F)$ = 0.0388 (for $I > 2\sigma(I)$), $wR_2(F^2)$ = 0.1004 (all data), residual electron density: 0.983/−0.732 e Å^{-3}.

CCDC reference number 188989.

See http://www.rsc.org/suppdata/dt/b3/b300823a/ for crystallographic data in CIF or other electronic format.

Acknowledgements

Support from the Danish Natural Science Council and COST project no. D21/0010/01 (C. J. M.) and a travel grant from Acta Chimica Scandinavica (M. N. M.) is gratefully acknowledged.

References

1 C. W. Hoganson and J. E. Penner-Hahn, *Biochemistry*, 1995, **34**, 1507–1512.
2 V. V. Barynin, M. M. Whittaker, S. V. Antonyuk, V. S. Lamzin, P. M. Harrison, P. J. Artymiuk and J. W. Whittaker, *Structure*, 2001, 725–738.
3 M. Atta, P. Nordlund, A. Åberg, H. Eklund and M. Fontecave, *J. Biol. Chem.*, 1992, **267**, 20682–20688; M. Hogbom, M. E. Andersson and P. Nordlund, *J. Biol. Inorg. Chem.*, 2001, 315–323.
4 V. J. Leveque, M. E. Stroupe, J. R. Lepock, D. E. Cabelli, J. A. Tainer, H. S. Nick and D. N. Silverman, *Biochemistry*, 2000, **39**, 7131–7137.
5 M. Sundaramoorthy, K. Kishi, M. H. Gold and T. L. Poulos, *J. Mol. Biol.*, 1994, **238**, 845–848.
6 *Manganese Redox Enzymes*, ed. V. L. Pecoraro, VCH Publishers, Inc., New York, 1992.
7 C. Su and E. H. Oliw, *J. Biol. Chem.*, 1998, **273**, 13072–13079; M. Hamberg, C. Su and E. Oliw, *J. Biol. Chem.*, 1998, **273**, 13080–13088.
8 L. Hörnsten, C. Su, A. E. Osbourne, U. Hellman and E. H. Oliw, *Eur. J. Biochem.*, 2002, **269**, 2690–2697.
9 D. M. Eichhorn and W. H. Armstrong, *J. Chem. Soc., Chem. Commun.*, 1992, 85–87.
10 Z. Shirin, V. G. Young, Jr. and A. S. Borovik, *Chem. Commun.*, 1997, 1968–1969; Z. Shirin, B. S. Hammes, V. G. Young, Jr. and A. S. Borovik, *J. Am. Chem. Soc.*, 2000, **122**, 1836–1837; R. Gupta, C. E. MacBeth, V. G. Young, Jr. and A. S. Borovik, *J. Am. Chem. Soc.*, 2002, **124**, 1136–1137.
11 An Fe(III)–OH distance of 1.89 Å was determined by EXAFS: C. J. McKenzie, R. Scarrow, unpublished results.
12 T. Howard, J. Tesler and V. J. DeRose, *Inorg. Chem.*, 2000, **39**, 3379–3385.
13 H. Iikura and T. Nagata, *Inorg. Chem.*, 1998, **37**, 4702–4711.
14 O. Horner, E. Anxolabéhère-Mallart, M.-F. Charlot, L. Tchertanov, J. Guilhem, T. A. Mattioli, A. Boussac and J.-J. Girerd, *Inorg. Chem.*, 1999, **38**, 1222–1232.
15 A. L. Nivorozhkin, E. Anxolabéhère-Mallart, P. Mialane, R. Davydov, J. Guilhem, M. Cesario, J.-P. Audière, J.-J. Girerd, S. Styring, L. Schussler and J.-L. Seris, *Inorg. Chem.*, 1997, **36**, 846–853.
16 O. Kahn, *Molecular Magnetism*, VCH, New York, 1993.
17 Bruker Analytical X-Ray Instruments Inc., Madison, WI, USA, 2000.
18 G. M. Sheldrick, University of Göttingen, Germany, 2001.
19 G. M. Sheldrick, SHELXTL: Structure Determination Programs, Version 5.10, Bruker Analytical X-Ray Instruments Inc., Madison, WI, USA, 1997.
20 A. L. Spek, *Acta Crystallogr., Sect. A*, 1990, **46**, C34.